Microbolometric responsivity analysis for focal plane array under pulsed voltage bias

XIQU CHEN*, LINGBO HE, CHAO FANG, QIANG LV
School of Electrical & Electronic Engineering, Wuhan Polytechnic University, Wuhan, China

The microbolometric voltage responsivity is theoretically obtained on the base of the thermal balance equation and the basic signal readout circuits for a typical microbolometer. The theoretical responsivity expression indicates that two vital factors to decide its value are the pulsed bias voltage and time. Some numerical calculations based on the theoretical voltage responsivity expression reveal the relationships between the microbolometric voltage responsivity and these two pulsed bias parameters. The pulsed bias parameters optimization for microbolometric focal plane array can be achieved on the theoretical analysis and these numerical calculations, which is potential for microbolometer arrays to their sensitive improvement.

(Received August 18, 2021; accepted April 8, 2022)

Keywords: Microbolometer, Focal plane array, Responsivity, Pulsed voltage bias, Infrared

1. Introduction

The typical microbolometer is normally connected to the readout integrated circuits in the silicon (Si) substrate under the sensor array in a practical focal plane array [1-4]. If the microbolometer is heated by a certain incident infrared irradiation power, its resistance must be changed for its thermal sensitivity [5-8]. The resistance changes of the microbolometer need to be converted into a photo-generated current signal by applying a bias voltage, and the photo-generated current can then be integrated onto a capacitor in the readout integrated circuits to form the voltage signal in response to the infrared irradiation power [9,10]. Ideally, the response voltage is directly proportional to the infrared irradiation power. The proportional coefficient of the response voltage and the infrared irradiation power is defined as the microbolometric voltage responsivity, and it is relating to several parameters such as the bias voltage, the thermal conductance, some thermoelectric parameters of the microbolometer, the photo-generated current integration capacitor and time, and so on, which is explained in the following part. In order to improve the thermal sensitive property of the microbolometric focal plane array, the relationship between the microbolometric responsivity and these key factors should be carefully investigated. Furthermore, the microbolometric responsivity should be accurately analyzed and discussed for the microbolometric focal plane array under pulsed bias in working condition because the microbolometric responsivity under pulsed bias is normally significantly different from that under constant bias, which is due to the operating temperature continuing increasement of the microbolometer during the pulsed bias period [11].

The photo-generated current responsivity of the microbolometer under pulsed voltage bias has been numerically calculated by P.W. Kruse [12], but its theoretical expression has not been given out by him. The photo-generated current responsivity expression under pulsed voltage bias is theoretically put forward in one of our published papers [13], however, it is approximatively based on some numerical calculations and not theoretically strict. The strict photo-generated current responsivity is theoretically deduced based on some detailed derivations in some of our published papers [14,15], but it is merely applicable to the microbolometer array under constant voltage bias. The microbolometric theoretical voltage responsivity analysis for focal plane array under pulse current bias is introduced in other two our published papers [16,17], but it can only be used to the responsivity analysis of the microbolometer under pulsed current bias. The voltage responsivity of the microbolometer under pulsed voltage bias is derived from a list of theoretical deduce processes in another of our published papers [18], nevertheless, it is too theoretically complex to be directly utilized for the optimization of the microbolometric responsivity. Thus, it is still a challenge to disclose the influences of the key factors on the microbolometric responsivity for the performance optimization of high-sensitive microbolometric focal plane arrays.

Because the joule heating power from the pulse voltage bias is significantly larger than the typical infrared power absorbed by the microbolometer, the operating temperature of the microbolometer under pulsed voltage bias is increased at a fast speed during the voltage bias pulse due to the joule heating power produced by the pulsed bias voltage. In consideration that the microbolometer resistance is a function of the microbolometer temperature, the microbolometric voltage responsivity should be carefully studied with the operating temperature changes of the microbolometer under pulsed

voltage bias. The voltage responsivity of the microbolometer under pulsed voltage bias relating to the microbolometric operating temperature changes is theoretically proposed in following part. The numerical simulations on the microbolometric voltage responsivity with the adjustment of the pulse bias voltage and time according to the proposed theoretical voltage responsivity of the microbolometer are introduced in Section 3, from which the affections on the microbolometric voltage responsivity caused by the pulse bias voltage and time can be directly observed. At last, conclusions are drawn in the Section 4.

2. Operating temperature and voltage responsivity

When a practical microbolometric focal plane array works, the thermal balance equation for the typical microbolometer in the array can be written as

$$c\frac{dT}{dt} = \frac{V_b^2}{R(T)} + P_a - g(T - T_s) \tag{1}$$

where c and g are the heat capacity and thermal conductance respectively of the microbolometer in its thermally isolated structure [19-21]. If the microbolometer is biased by a pulse voltage V_b, its resistance at the operating temperature T at some time t during the voltage bias pulse is $R(T)$ with a constant Si substrate temperature T_s. Then, the microbolometric resistance change resulted from the microbolometric temperature increasement due to the absorbed infrared irradiation power P_a can be looked as a thermal-sensitive resistance response perturbation, because the absorbed infrared power P_a is far smaller than the voltage bias power $\frac{V_b^2}{R(T)}$.

While other microbolometric characteristic parameters are constant, the operating temperature of the microbolometer is determined by the pulse voltage bias power. Ignoring the absorbed infrared power P_a, the thermal balance equation (1) can be changed into

$$c\frac{dT}{dt} = \frac{V_b^2}{R(T)} - g(T - T_s) \tag{2}$$

In consideration that the thermoelectric property of the microbolometer has semiconductor characteristics, the resistance of the microbolometer such as vanadium oxides can be expressed as

$$R(T) = R_0 e^{\frac{E_g}{2kT}} \tag{3}$$

where R_0 is a constant, E_g is the bandgap of the microbolometer materials, and k is the Boltzmann constant. From Eqs. (2) and (3), we can get

$$\frac{dT}{dt} + \frac{1}{c/g}T = \frac{1}{c/g}T_s + \frac{V_b^2}{cR_0} \times e^{-\frac{E_g}{2kT}} \tag{4}$$

The theoretical operating temperature expression for the microbolometer during pulse voltage bias period cannot be derived directly from Eq. (4), but it can be gotten through the curve fitting based on the numerically calculated operating temperature data from the above equation.

In a similar way, the thermal balance equation for the microbolometer during the zero-bias period is

$$\frac{dT}{dt} + \frac{1}{c/g}T = \frac{1}{c/g}T_s \tag{5}$$

From Eq. (5), the operating temperature of the microbolometer during the zero-bias period can be derived as

$$T(t) = T_s + [T(t_0) - T_s]e^{-\frac{g}{c}(t - t_0)} \tag{6}$$

where $T(t_0)$ is the microbolometric initial temperature at the beginning time t_0 of the zero-bias period.

A complete video frame time of a practical microbolometric focal plane array can be divided into two periods: The first is the pulse voltage bias period, during which the operating temperature rises, and the second is the zero-bias period, during which the operating temperature falls. Because the video frames of the focal plane array are successive in turn, the operating temperature changes of the microbolometer must contain a series of rising and falling processes to form steady cycles finally [18], of which the schematic diagram is illustrated Fig. 1. The final steady cycling operating temperatures are between the constant low temperature T_l and the constant high temperature T_h.

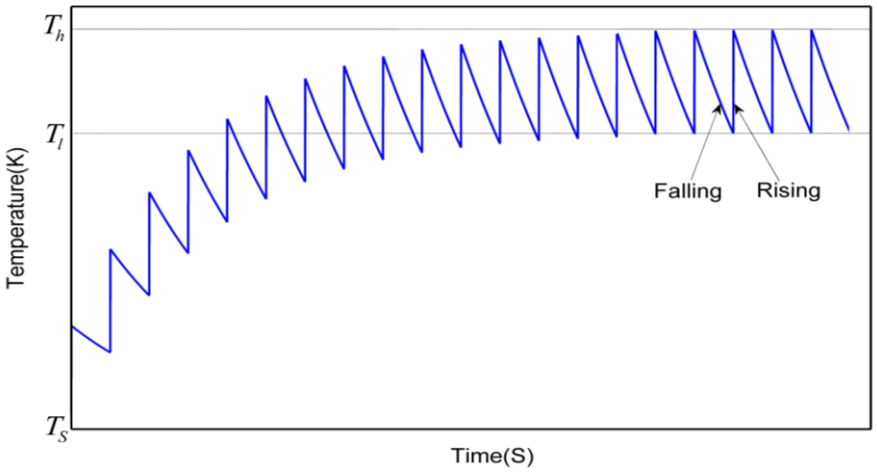

Fig. 1. The operating temperature change schematic diagram of the microbolometer (color online)

The typical steady temperature change period is numerically calculated and simulated based on Eqs. (4) and (6) to be shown in Fig. 2, for which the characteristic parameters of the microbolometer are listed in Table 1, where Δt_1 is the pulse voltage bias time, Δt is the video frame time, and α is the microbolometer temperature coefficient of resistance as

$$\alpha = \frac{\Delta R(T)}{R(T)\Delta \mathrm{T}} = -\frac{E_g}{2kT^2} \tag{7}$$

From Fig. 2, it can be found that the operating temperature rising of the microbolometer during the pulse voltage bias period is very rapid and the operating temperature falling of the microbolometer during the zero bias period is relatively gentle in a negative exponential function of time. The corresponding operating temperature rising curve of the microbolometer during the pulse voltage bias period is shown in Fig. 3, which is completely linear within the extremely short pulse voltage bias time.

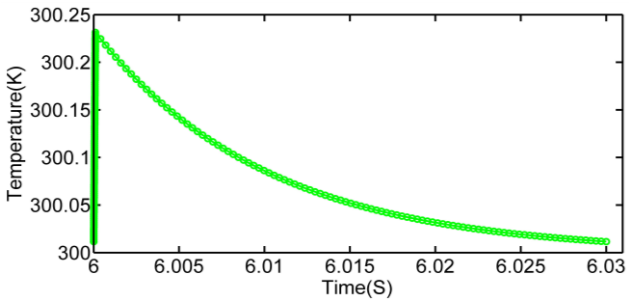

Fig. 2. The typical steady period temperature change curve of the microbolometer (color online)

Table 1. Characteristic parameters of the microbolometer

Parameter	Value
$R(300)$	20KΩ at temperature 300K
T_S	300K
c	1×10^{-9}J/K
g	1×10^{-7} W/K
α	-0.02 at temperature 300K
Δt_1	100μsec
Δt	30msec
V_b	0.21V

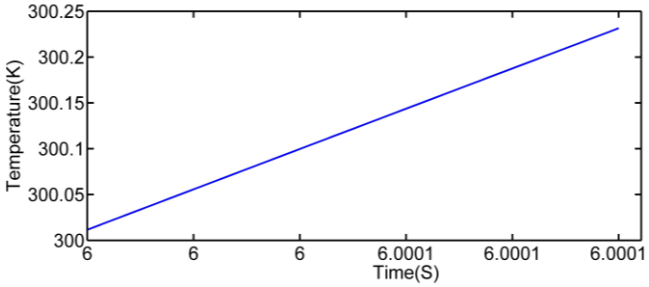

Fig. 3. The steady operating temperature rising curve of the microbolometer during pulse voltage bias period (color online)

From above analyses, the operating temperature rising expression during the pulse voltage bias period can be processed as

$$T(t) = T_l + \frac{T_h - T_l}{100\times10^{-6}} t \cdot \ (0 \le t \le \Delta t_1) \tag{8}$$

Through linear fitting, the above equation can be expressed as

$$T(t) = T_l + \frac{V_b^2}{cR(T_l)} t \cdot (0 \le t \le \Delta t_1) \tag{9}$$

Considering that the operating temperature changing curve is continual with Eqs. (6) and (9), we can get

$$T_l = T_S + \frac{\Delta t_1 V_b^2}{cR(T_l)[e^{\frac{g}{c}(\Delta t - \Delta t_1)} - 1]} \tag{10}$$

If the bias power $\frac{V_b^2}{R(T)}$ is not too large resulting an obvious temperature shift between T_s and T_l, the microbolometer resistance $R(T_l)$ can be treated as $R(T_S)$. Thus, the operating temperature rising expression during the pulse voltage bias period ($0 \le t \le \Delta t_1$) can be changed into

$$T(t) = T_S + \frac{\Delta t_1 V_b^2}{cR(T_S)[e^{\frac{g}{c}(\Delta t - \Delta t_1)} - 1]} + \frac{V_b^2}{cR(T_S)} t \tag{11}$$

The typical infrared response signal readout structure of integrated circuits for the microbolometer is shown in Fig. 4, in which R_b has the same thermoelectric characteristics as the microbolometer $R(T)$ but not exposed to infrared radiation and A is an integrated operational amplifier. When the pair of bias controlling switches M_1 and M_2 are turned on after the reset switch M_3 discharges all the electric charges on the integration capacitor C, the photo-generated current I_p is integrated onto the integration capacitor. Because the microbolometric temperature change caused by the absorbed infrared power can be treated as a small perturbation on the thermal equilibrium of the microbolometer at any time during pulse voltage bias period, the microbolometric thermal balance equation (1) in thermal equilibrium can be expressed as

$$0 = \frac{V_b^2}{R(T)} + P_a - g(T - T_s) \tag{12}$$

From Eq. (12), the microbolometric temperature responsivity can be derived as

$$\frac{dT}{dP_a} = \frac{1}{g + \frac{V_b^2}{R(T)}\alpha} \tag{13}$$

In addition, the microbolometric photo-generated current responsivity is

$$R_I = \frac{dI_p}{dT} \times \frac{dT}{dP_a} = \frac{d\frac{V_b}{R(T)}}{dT} \times \frac{dT}{dP_a} = -\frac{V_b \alpha}{R(T)} \frac{dT}{dP_a} \tag{14}$$

From Eqs. (13) and (14), it can be gotten

$$R_I = -\frac{V_b \alpha}{R(T)g + V_b^2 \alpha} \tag{15}$$

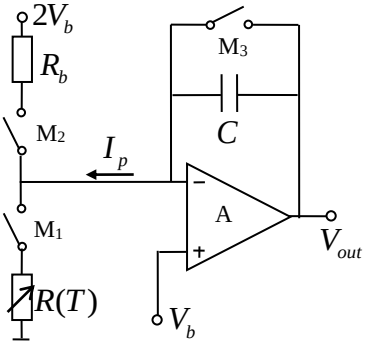

Fig. 4. The infrared response signal readout integrated circuits structure for the microbolometer

If the absorbed infrared irradiation power P_a is invariant during the pulse voltage bias time Δt_1, the output voltage of the integrated operational amplifier in Fig. 4 is

$$V_{out} = \frac{1}{C}\int_0^{\Delta t_1} -\frac{V_b \alpha P_a}{R(T)g + V_b^2 \alpha} dt \tag{16}$$

Thus, the microbolometric voltage responsivity is

$$R_v = \frac{V_{out}}{P_a} = \frac{1}{C}\int_0^{\Delta t_1} -\frac{V_b \alpha}{R(T)g + V_b^2 \alpha} dt \tag{17}$$

With Eqs. (3) and (7), the above equation can be transformed into

$$R_v = \frac{1}{C}\int_0^{\Delta t_1} \frac{V_b E_g}{2kT^2 g R_0 e^{\frac{E_g}{2kT}} - V_b^2 E_g} dt \tag{18}$$

Because the operating temperature expression during the pulse voltage bias period is theoretically given out as Eq. (11), Eq. (18) can be looked as the theoretical expression of the microbolometric voltage responsivity with Eq. (11).

3. Microbolometric voltage responsivity simulation

From Eqs. (11) and (18), it can be found that the microbolometric voltage responsivity can be decided by two adjustable pulse bias parameters Δt_1 and V_b with other constant thermal and electronic parameters such as *c*, *g*, T_s, *C*, E_g and R_0. When the pulse voltage V_b is adjusted from 0.1V to 0.5V, the integration capacitor C is equal to 10pF, and other characteristic parameters of the

microbolometer are unchanged as listed in Table 1, the corresponding microbolometric voltage responsivity changing curve is numerically simulated and shown in Fig. 5. In consideration that large pulse voltage must result in large bias power dissipation and output noise [11,14], the pulse voltage should be controlled below the first microbolometric voltage responsivity extreme point to get an appropriate output responsivity with low output noise. The pulse voltage is controlled from 0.1V to 0.3V, and the microbolometric voltage responsivity simulation results is shown in Fig. 6. The microbolometric voltage responsivity can reach about 5×10^{7} V/W while the bias voltage is 0.25V, which is big enough for the microbolometric infrared response.

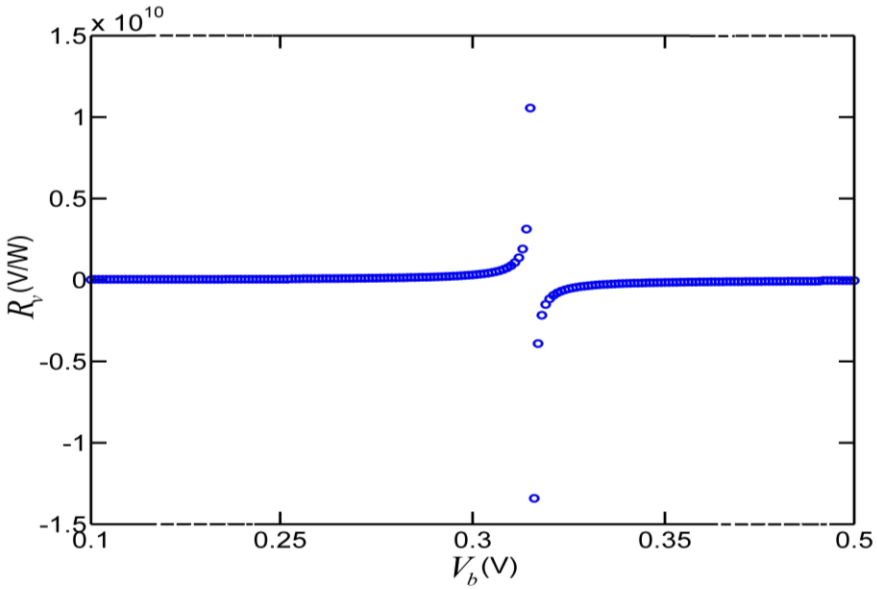

Fig. 5. The microbolometric voltage responsivity numerical simulation curve with the pulse voltage adjusted from 0.1 to 0.5V (color online)

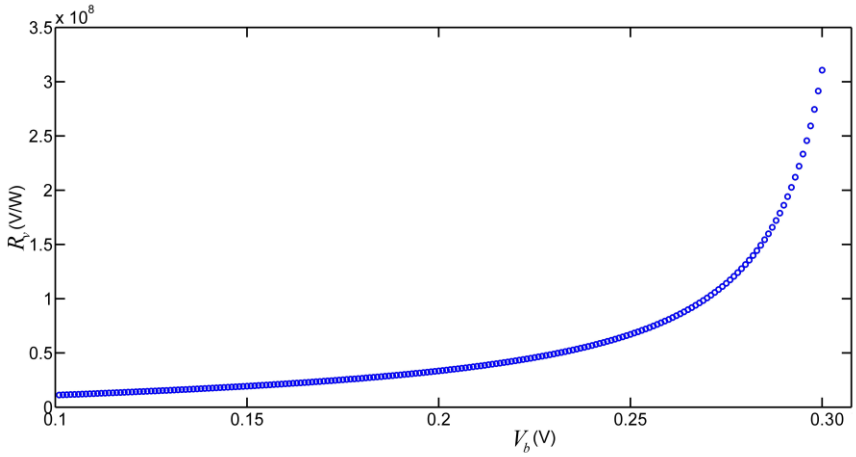

Fig. 6. The microbolometric voltage responsivity numerical simulation curve with the pulse voltage adjusted from 0.1 to 0.3V (color online)

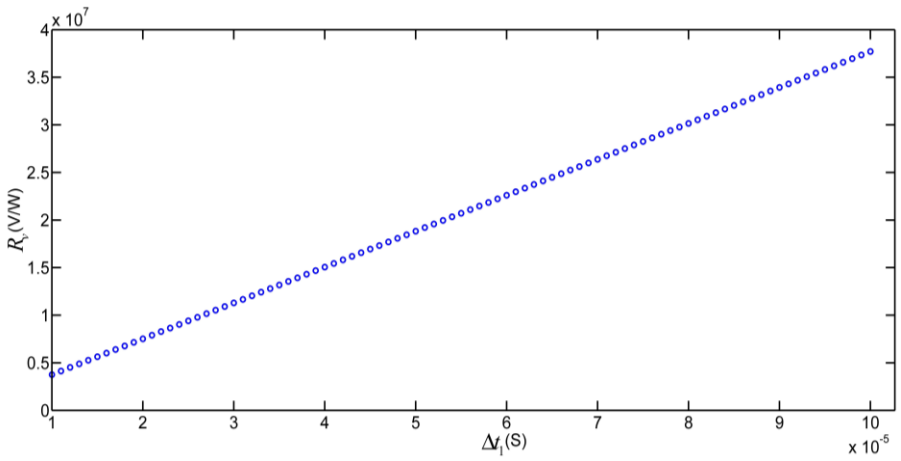

Fig. 7. The microbolometric voltage responsivity numerical simulation curve with the pulse bias time adjusted from 10 to 100μsec (color online)

At the same time, the microbolometric voltage responsivity numerical simulations are also carried out with the pulse bias time adjusted from 10μsec to 100μsec. The microbolometric voltage responsivity numerical simulation curve is shown in Fig. 7, for which the bias voltage is optimized to be 0.21V and the other microbolometric characteristic parameters are the same as those for the numerical simulations of Fig. 6. It can be found that the relationship between the microbolometric voltage responsivity and the pulse bias time is almost completely linear, which indicates that the increasement of the pulse bias time can produce the improvement of the microbolometric voltage responsivity.

Because the integration time of the photo-generated current is equal to the pulse bias time, the increasement of the pulse bias time can effectively suppress the output noise of the microbolometer [14,22]. Combined with the above analysis, the pulse bias time should be as large as possible to obtain the maximum output signal-to-noise ratio of the microbolometric response, which is often constrained by the operating mode and infrared signal readout structure of readout integrated circuits. After the maximization of the pulse bias time, the bias voltage can be optimized to get an appropriate microbolometric voltage responsivity according to the numerical simulations for Figs. 5 and 6.

4. Conclusions

The microbolometric responsivity for focal plane array under pulsed voltage bias is theoretically analyzed and numerically calculated. The microbolometric responsivity expression is theoretically given out for the first time and reveals two key adjustable pulse bias parameters the pulse bias time and voltage. On the base of the theoretical expression, the microbolometric responsivity curves are numerically simulated with the adjusted pulse bias voltage and time within certain ranges respectively. The numerical simulation results imply an effective optimization method for high signal-to-noise ratio microbolometric focal plane arrays, which was verified with some prototypes of microbolometer arrays in our laboratory. It is worthwhile to note that the starting microbolometer resistance $R(T_l)$ is treated as the microbolometer resistance at substrate temperature $R(T_S)$, which is inapplicable to the microbolometric focal plane array with large pulse voltage and bias time. The microbolometric responsivity theoretical analysis and numerical calculations for focal plane array under pulsed voltage bias with large bias voltage and time will be published in another paper, which is only suitable for few infrared applications.

Acknowledgments

This work was supported by China Hubei Provincial Department of Education (ID: D20191605) and China Hubei Provincial Science & Technology Department (ID: 2019CFB813).

References

[1] X. Yi, S. Chen, Y. Wang, B. Xiong, H. Wang International Journal of Infrared and Millimeter Waves **23**(12), 1699 (2002).
[2] H. Jerominek, M. Renaud, N. R. Swart, F. Picard, T. D. Pope, M. Levesque, M. Lehoux, G. Bilodeau, M. Pellettier, D. Audet, P. Lambert, Proc. SPIE. Int. Soc. Opt. Eng. **2882**, 111 (1996).
[3] J. Lv, L. Que, L. Wei, Y. Zhou, IEEE Sens. J. **14**(5), 1533 (2014).
[4] H. Wang, X. Yi, G. Huang, J. Xiao, X. Li, S. Chen, Infrared Phys. Technol. **45**(1), 53 (2004).
[5] R. A. Wood, N. A. Foss, Laser Focus World **29**(6), 101 (1993).
[6] X. Chen, C. Fang, Q. Lv, Z. Shang, Optik **188**, 110 (2019).
[7] C. C. Hsieh, C. Y. Wu, F. W. Jih, T. P. Sun, IEEE Trans. Circuits Syst. Video Technol. **7**(4), 594 (1997).
[8] X. Yi, S. Chen, Y. Wang, J. Infrared Millim. Terahz. Waves **23**(12), 1699 (2002).

[9] X. Chen, J. Infrared Millim. Terahz. Waves **31**(5), 566 (2010).
[10] H. Wang, X. Yi, J. Lai, International Journal of Infrared and Millimeter Waves **26**(5), 751 (2005).
[11] R. A. Wood, in: P. W. Kruse, D. D. Skatrud (Eds.), Uncooled Infrared Imaging Systems and Arrays, Academic Press, Smith, New York, 1997, pp. 59–67.
[12] P. W. Kruse, Proc. SPIE Infrared Technology XXI **2552**(8), 556 (1995).
[13] X. Chen, Q. Lv, X. Yi, Optik, **122**(23), 2143 (2011).
[14] X. Chen, H. Zhao, C. Fang, Q. Lu, L. Chen, Optik **219**, 165118 (2020).
[15] X. Chen, C. Fang, Q. Lv, R. Yang, Optik **170**, 452 (2018).
453
[16] X. Chen, Y. Tan, C. Fang, Q. Lv, Optik **231**, 166445 (2021).
[17] X. Chen, C. Fang, Q. Lv, Optik **177**, 21 (2019).
[18] X. Chen, Q. Lv, Opt. Eng. **54** (6), 0631051 (2015).
[19] S. Tohyama, M. Miyoshi, S. Kurashina et al., Opt. Eng. **45**(1), 1 (2006).
[20] H. Wang, X. Yi, S. Chen, J. Infrared Millim. Waves **23**(2), 99 (2004).
[21] C. Chen, X. Yi, J. Zhang, B. Xiong, International Journal of Infrared and Millimeter Waves **22**(1), 53 (2001).
[22] X. Chen, B. Liu, C. Fang, Q. Lv, Optik **240**, 166910 (2021).

*Corresponding author: cxqdhl@sina.cn